PHYSICAL REVIEW B **86**, 241405(R) (2012)

Designer reflectors using spoof surface plasmons in the terahertz range

Jingbo Liu, Rajind Mendis, and Daniel M. Mittleman
Department of Electrical and Computer Engineering, MS 378, Rice University, Houston, Texas 77251-1892, USA
(Received 17 September 2012; revised manuscript received 23 October 2012; published 21 December 2012)

We show that spoof surface plasmons can be used to control the reflection of terahertz radiation at the output facet of a parallel-plate waveguide. Using a periodic groove pattern on the output face, reflectivity approaching 100% can be achieved within a limited spectral range. Unlike the conventional geometry for plasmon-enhanced transmission, this approach enables a unique method for studying the coupling between the guided mode and the surface plasmon through angle-dependent measurement of the plasmon-mediated reflection. A simple model incorporating the surface plasmon coupling to the waveguide mode can adequately explain all of the observed phenomena, including the observed Goos-Hänchen shift in the reflected beam.

DOI: 10.1103/PhysRevB.86.241405 PACS number(s): 73.20.Mf, 42.79.Gn, 42.25.Gy

A metal surface which has been patterned on a subwavelength scale can support a surface wave known as a spoof surface plasmon.[1] Spoof surface plasmons (SSPs) are an important class of plasmonic excitation, as their properties can be controlled through design of the surface structure.[2,3] This idea is particularly relevant in the terahertz region of the spectrum, where metallic conductivities are typically very high and consequently surface waves on smooth metals are weakly bound.[4–7] The concept of the SSP has opened a number of possibilities for optics in the terahertz range. Examples include channeling of waves into a subwavelength volume[8,9] or through a subwavelength aperture,[10–13] and control of both the spatial mode profile and the absolute transmission from the output facet of a terahertz quantum cascade laser.[14]

In contrast to enhanced transmission, the idea of using SSPs for enhanced *reflection* has not previously been discussed. Although it is clear that a designer SSP can either enhance or diminish the transmission at a given frequency, the advantages of the reflection geometry for elucidating the surface plasmon coupling mechanism has not yet been described. Here, we show that a reflection geometry has a unique advantage over the conventional transmission configuration. By structuring the output facet of a metal waveguide,[15] one can inhibit the coupling of the guided mode into free space and therefore greatly enhance the reflection of the wave back into the waveguide. With a careful design of the structure at the waveguide output facet, reflection coefficients near 100% within a limited spectral bandwidth can be engineered. Unlike in most earlier studies involving SSP enhanced transmission, this situation lends itself to an investigation of the angle dependence of the enhanced reflection. This allows us to study the coupling between the guided mode and the SPP explicitly. We develop a simple model to describe this coupling, and show that it is adequate to explain all of the observations, including the observed Goos-Hänchen shift in the reflected beam.

Our approach relies on a parallel-plate waveguide (PPWG), a common platform for terahertz applications including pulse generation,[16] signal processing,[17] spectroscopy,[18] imaging,[19,20] and sensing.[21,22] Nearly all of these examples make use of the dominant TEM waveguide mode, for which the Ohmic loss is low and the group-velocity dispersion is negligible.[23] It has been shown that TEM waves propagating inside a PPWG are not perfectly impedance matched to free space. As a result, when a propagating TEM wave reaches an abrupt termination (i.e., an output facet), some fraction of the wave's energy is reflected back into the waveguide. For a large plate spacing $b > \lambda$, this reflection is quite small; for b comparable to or smaller than λ, the reflection coefficient at this interface increases approximately linearly with increasing wavelength.[24] Structuring the output facet can allow us to control aspects of this impedance matching. In earlier experiments involving semiconductor lasers,[14,15] the goal was to *maximize* the power flow out of the waveguide and optimize the spatial mode of the output beam. However, it is also possible to *minimize* this power flow, so that the wave energy is reflected back into the waveguide at a selected frequency. By choosing the appropriate geometrical parameters, we can design a high reflector.

To explore this situation, we fabricate a series of several different waveguides from aluminum plates. In each, a pattern of five identical straight grooves are cut into the output facet of both the upper and lower waveguide plates, parallel to the output aperture. Figure 1(a) illustrates a cross section of a pattern of periodic grooves on the output facet, adjacent to the waveguide's exit aperture. In our fabricated structures, the grooves are rectangular in cross section, with a width (w) of 152 μm. The plate spacing (b), groove depth (h), periodic spacing (d), and the distance from the first groove to the waveguide aperture edge (L) are varied to tune the frequency and strength of the surface plasmon coupling.[1,5,14,15] Figure 1(b) shows a perspective rendering of an assembled waveguide structure, with the grooves visible on the upper and lower plates on the output facet. The red line indicates one possible incident beam path in the x-z plane (the waveguide plane), reflecting from the output aperture at an angle θ relative to the output facet normal. Prior to fabrication, we fine-tune the structure using finite element method (FEM) simulations.[25] Figures 1(c) and 1(d) show simulations of a PPWG with a particular groove pattern for normal incidence, $\theta = 0$. These two simulations show the results at the design frequency (197 GHz) and at a frequency away from it (225 GHz). We observe that at the design frequency [Fig. 1(c)] most of the wave energy is confined in the near field of the output aperture and is reflected back into the waveguide. The wave intensity inside the waveguide is enhanced by the interference of the

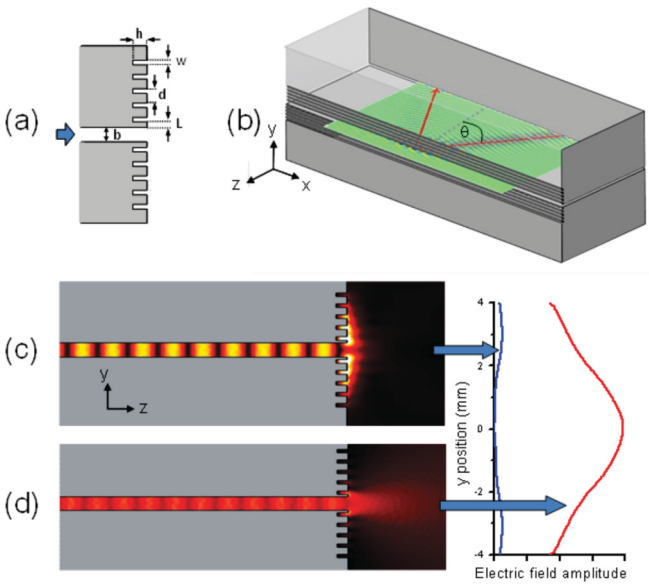

FIG. 1. (Color) (a) Schematic cross section of the PPWG with five grooves cut into the output facet on each plate. Geometrical parameters b, h, w, d, and L are defined as shown. (b) Perspective drawing of the assembled waveguide. The wave shown in the simulation, with superposed red lines, indicates one possible beam path, propagating inside the waveguide (in the x-z plane) and reflecting off of the structured output facet at an angle θ. (c) and (d) Simulations based on the finite element method, showing a cross section of a waveguide with a field propagating at $\theta = 0$. In (c), the wave frequency (197 GHz) equals the design frequency of the groove reflector, while in (d) the wave frequency (225 GHz) is far from the design frequency. The plot at the right shows the field amplitudes at a distance of 3 mm from the end of the waveguide, from these two simulations.

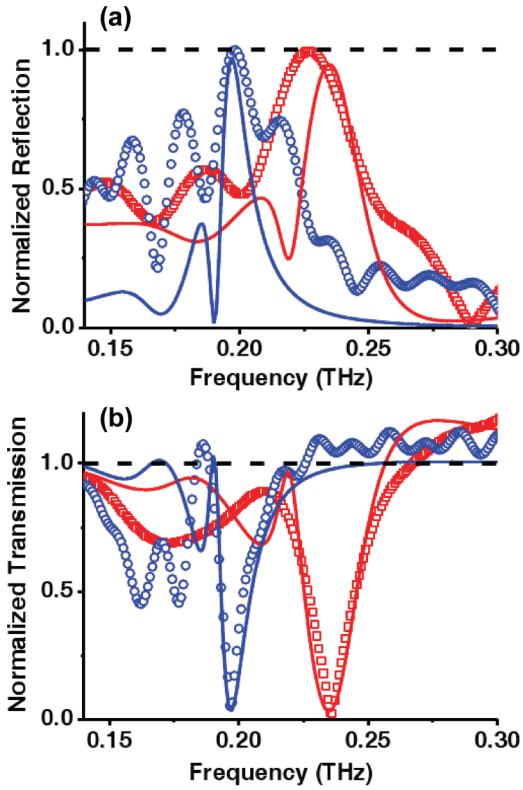

FIG. 2. (Color) (a) Measured (symbols) and simulated (solid curves) normalized reflection spectra for two different waveguides, with design frequencies of 197 (blue) and 234 GHz (red). (b) Measured and simulated normalized transmission spectra for the same two waveguides as in (a). In both cases the angle $\theta = 0$. The waveguide structural parameters [defined in Fig. 1(a)] are $w = 152$, $b = 600$, $L = 100$, $d = 475$, and $h = 274$ for the blue data points, and $w = 152$, $b = 200$, $L = 228$, $d = 457$, and $h = 205$ for the red data points. All units are microns.

incident and reflected waves, and no propagating wave is observed exiting the waveguide to the right. In comparison, in the off-resonant situation [Fig. 1(d)] nearly all of the power in the incoming wave is coupled out into free space.

Figure 2 shows typical experimental transmission and reflection spectra, for two different groove patterns measured at $\theta = 0$. The reflection spectra [Fig. 2(a)] are measured using a beam splitter placed before the input facet of the waveguide, so that a true $\theta = 0$ reflection is obtained. These spectra are normalized to the reflection that is obtained when a mirror is pressed directly against the waveguide's output facet, which gives an almost perfect reflection of all spectral components at this facet.[24] The transmission spectra [Fig. 2(b)] are measured by collecting the radiation emerging through the output facet. These spectra are normalized to the measured transmission spectra through an unmodified waveguide (i.e., with no grooves) of identical dimensions. In both cases, a strong modification of the spectrum is observed at the design frequency, where the reflected power approaches 100%. The interaction of the spoof surface plasmon mode and the PPWG TEM mode becomes dominant at this frequency. The simulated results (solid curves) are in reasonable agreement with our measurements. The agreement is somewhat poorer for the reflection measurements for experimental reasons: to achieve a normal-incidence reflection, we use a beam splitter which introduces etalon modulation superimposed on the measured terahertz signal. The precise normalization of these etalon effects is challenging, resulting in some deviations from the simulated results.

In addition to the designed peak in the reflectivity, we also observe other modifications to the spectrum induced by the grooves. As noted above, for a small plate spacing the transmission can drop well below 100% even for an ungrooved waveguide, due to impedance mismatch of the TEM mode with empty space. (We note that the relevant impedance in the waveguide is not simply the wave impedance as defined by the ratio of the electric-field magnitude to the magnetic-field magnitude.[24]) At frequencies away from the design frequency, it is possible for our groove pattern to enhance the transmission out of the waveguide compared to the waveguide without grooves,[15] leading to an observed transmission spectrum that exceeds 100%. This effect is observed both experimentally and in the calculations, most prominently for the smaller plate spacing (red symbols and red curve).

A unique aspect of this reflection geometry is the ability to probe the interaction between the guided wave and the spoof surface plasmon by varying the angle of the incident wave. In order to perform angle-dependent measurements, we fabricate a series of waveguides, each with an identical set

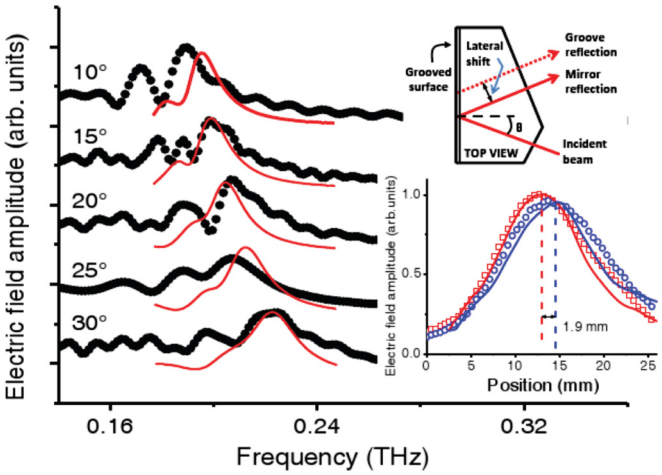

FIG. 3. (Color) Measured (black symbols) and simulated (red curves) reflection spectra as a function of frequency for several different angles θ. Each spectrum was measured on a different device, but all of the devices have the same nominal values for all of the geometrical parameters indicated in Fig. 1(a), and therefore the same value of ω_0 (191 GHz). Upper inset: a typical waveguide schematic, indicating the tilted surfaces designed so that the beam enters and exits the waveguide through a surface orthogonal to its wave vector. The diagram also indicates the lateral shift of the reflected beam. Lower inset: typical data for one case, with $\theta = 20°$. The red symbols represent the spatial profile of the beam reflected from a mirror pressed against the grooved surface, while the blue symbols represent the SSP-mediated reflection. The lateral shift of 1.9 mm between the beam centroids is consistent with numerical simulations of the two situations (red and blue solid curves).

of grooves but with an angled facet on the input side so that the input and reflected waves both pass through a waveguide facet that is normal to the k vector (as illustrated in the upper inset to Fig. 3). These angled waveguides are all designed to have a reflection maximum (at $\theta = 0$) at 191 GHz. As shown in Fig. 3, the frequency of the maximum reflection blueshifts with increasing angle θ, consistent with three-dimensional (3D) numerical simulations (red curves).

We also note that, as the incident angle increases, we observe a decrease in the peak reflectivity, from almost 99% at 10° to only 84% at 30°. This can be understood as follows: when the incident wave has a k-vector component parallel to the groove direction [the x axis in Fig. 1(b)], part of the energy can couple into a groove waveguide mode propagating along the groove axes. This mode, an analog of the channel plasmon,[26,27] can lead to energy loss for the reflected wave.

It is clear from these data that there must be an interaction between the guided mode inside the waveguide and the spoof surface plasmon mode on the output facet. We employ a model in which this interaction is described by the difference between two orthogonal wave-vector components. We represent this wave-vector difference by κ, defined as $\kappa = k_{W,z} - k_{\mathrm{SSP},y}$. Here $k_{W,z}$ is the z component of k_W (the wave vector of the TEM mode inside the waveguide), and is given by $k_{W,z} = (\omega/c)\cos\theta$. $k_{\mathrm{SSP},y}$ is the y component of the wave vector of the SSP at the design frequency for maximum reflectivity at $\theta = 0$. Since the design frequencies for our devices correspond to wavelengths that are large compared to the periodicity of the structure, $k_{\mathrm{SSP},y}$ is approximately given by ω_0/c, where ω_0 is the design frequency.[5] Thus, we find

$$\kappa = (\omega/c)\cos(\theta) - \omega_0/c. \tag{1}$$

We then assume that the amplitude reflection coefficient $r(\omega,\theta)$ at the waveguide output facet can be written in the form

$$r(\omega,\theta) = A(\kappa^2)e^{i\Phi(\kappa)}, \tag{2}$$

where $A(x)$ is a line shape function and $\Phi(x)$ is a phase function, both of which are unknown functions depending on κ as shown. The angle dependence of the frequency of the reflectivity maximum can then be derived by setting the partial derivative $\partial A/\partial\omega$ equal to zero, which immediately yields

$$\nu_{\mathrm{peak}} = \nu_0/\cos(\theta). \tag{3}$$

The measured peak frequencies are shown in Fig. 4(a), along with a plot of Eq. (3) (with no adjustable parameters) and also the results of FEM simulations, all showing good agreement.

The coupling between two orthogonal wave-vector components [Eq. (1)] can have important implications that are revealed by studying the angle dependence of the reflection. For example, this coupling introduces a lateral shift in the

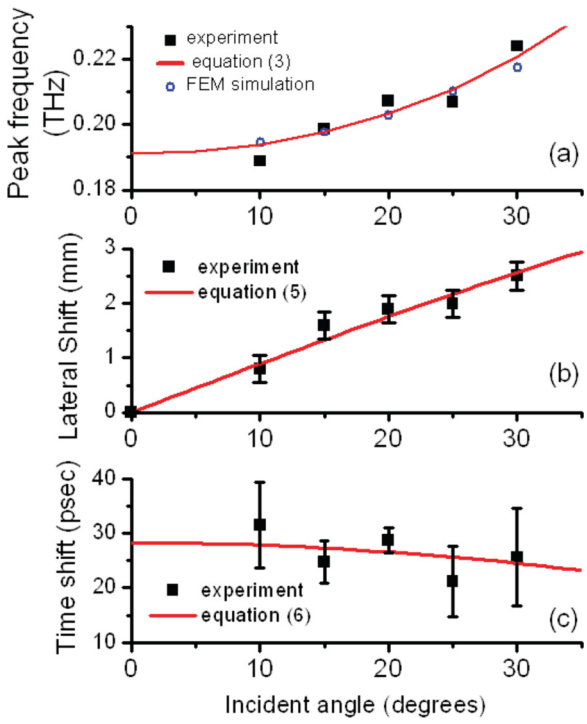

FIG. 4. (Color) (a) The black squares show the measured frequency of maximum reflection as a function of the angle of incidence. The blue circles show the results from 3D numerical simulations, while the red solid curve shows a plot of Eq. (3), with no adjustable parameters. (b) The lateral shift of the beam as a function of angle of incidence. The solid red curve is a plot of Eq. (5) with one fit parameter. (c) The temporal shift of the reflected beam (relative to that of a mirror reflection) as a function of angle of incidence. The solid red curve is a plot of Eq. (6) with no adjustable parameters. In all three cases shown here, the data are consistent with our model predictions.

position of the reflected beam. This lateral displacement Δ is reminiscent of the Goos-Hänchen effect, especially in cases where the reflecting medium is metallic.[28–30] Both effects can be explained as resulting from the propagation of an evanescent wave parallel to the interface. However, in the usual Goos-Hänchen effect the wave vector of the evanescent wave lies in the plane of incidence, whereas in our case the reflectivity is mediated by the wave-vector component perpendicular to the plane of incidence. The lower inset of Fig. 3 shows a typical result, comparing the output beam position (at the frequency of maximum reflection) from a mirror reflection to that from the grooves alone. For an incident Gaussian beam of size ~1.5 cm, we observe a lateral shift of a few millimeters associated with the SSP coupling. The solid lines show the corresponding FEM simulations. As noted previously,[31] the magnitude of Δ is very generally related to the phase of the reflection coefficient according to

$$\Delta = -\frac{1}{k}\frac{\partial \Phi}{\partial \theta}. \tag{4}$$

Applying this result to Eqs. (1) and (2), we find

$$\Delta = \Delta_0 \sin(\theta), \tag{5}$$

where Δ_0 is a fit parameter related to the form of $\Phi(\kappa)$. Over the range of our angular measurements, this description is in good agreement with our observations [Fig. 4(b)].

Finally, associated with a Goos-Hänchen-like spatial shift, one also expects a phase shift between the wave reflected from a mirror and from the SSP reflection. From our measurements, we extract the frequency derivative of the spectral phase difference between sample and reference measurements, in order to express the result as a time shift for each angle θ. Our model predicts that this time shift should be given by[31]

$$\delta t = \frac{\partial \Phi}{\partial \omega} = \delta t_0 \cos(\theta). \tag{6}$$

Here δt_0 is the time shift at normal incidence, which can be extracted from the temporal wave forms used to create Fig. 2. With no fit parameters, this prediction is consistent with the time shifts extracted from the angle-dependent measurements, as shown in Fig. 4(c).

In conclusion, we have demonstrated that spoof surface plasmons can be used to design the reflectivity at a waveguide output facet. A reflection coefficient close to 100% can be designed and experimentally observed within a limited spectral range. With our approach, it is possible to explore the coupling between the guided mode and the SSP mode in a manner which has previously been inaccessible to experiments. We propose a model for the reflectivity which incorporates the coupling between orthogonal wave-vector components. This model explains all of the observed angle-dependent phenomena associated with this SSP-mediated reflection.

[1] J. B. Pendry, L. Martin-Moreno, and F. J. Garcia-Vidal, Science **305**, 847 (2004).
[2] E. Ozbay, Science **311**, 189 (2006).
[3] Z. Fu, Q. Q. Gan, Y. J. Ding, and F. J. Bartoli, IEEE J. Sel. Top. Quantum Electron. **14**, 486 (2008).
[4] K. Wang and D. M. Mittleman, Nature (London) **432**, 376 (2004).
[5] C. R. Williams, S. R. Andrews, S. A. Maier, A. I. Fernandez-Dominguez, L. Martin-Moreno, and F. J. Garcia-Vidal, Nat. Photonics **2**, 175 (2008).
[6] W. Q. Zhu, A. Agrawal, and A. Nahata, Opt. Express **16**, 6216 (2008).
[7] L. F. Shen, X. D. Chen, and T. J. Yang, Opt. Express **16**, 3326 (2008).
[8] S. A. Maier, S. R. Andrews, L. Martin-Moreno, and F. J. Garcia-Vidal, Phys. Rev. Lett. **97**, 176805 (2006).
[9] J. K. Yang, C. S. Kee, and J. W. Lee, Opt. Express **19**, 20199 (2011).
[10] A. Agrawal, H. Cao, and A. Nahata, Opt. Express **13**, 3535 (2005).
[11] J. W. Lee, M. A. Seo, J. Y. Sohn, Y. H. Ahn, D. S. Kim, S. C. Jeoung, C. Lienau, and Q. H. Park, Opt. Express **13**, 10681 (2005).
[12] M. A. Seo, A. J. L. Adam, J. H. Kang, J. W. Lee, S. C. Jeoung, Q. H. Park, P. C. M. Planken, and D. S. Kim, Opt. Express **15**, 11781 (2007).
[13] D. S. Bulgarevich, M. Watanabe, and M. Shiwa, New J. Phys. **14**, 053001 (2012).
[14] N. Yu, Q. J. Wang, M. A. Kats, J. A. Fan, S. P. Khanna, L. H. Li, A. G. Davies, E. H. Linfield, and F. Capasso, Nat. Mater. **9**, 730 (2010).
[15] N. Yu, J. Fan, Q. J. Wang, C. Pflügl, L. Diehl, T. Edamura, M. Yamanishi, H. Kan, and F. Capasso, Nat. Photonics **2**, 564 (2008).
[16] H. Cao, R. A. Linke, and A. Nahata, Opt. Lett. **29**, 1751 (2004).
[17] D. G. Cooke and P. U. Jepsen, Opt. Express **16**, 15123 (2008).
[18] J. S. Melinger, S. S. Harsha, N. Laman, and D. Grischkowsky, J. Opt. Soc. Am. B **26**, A79 (2009).
[19] M. A. Musheinesh, C. J. Divin, J. A. Fessler, and T. B. Norris, Opt. Express **17**, 13663 (2009).
[20] J. Liu, R. Mendis, and D. M. Mittleman, Appl. Phys. Lett. **100**, 031101 (2012).
[21] M. Nagel, M. Forst, and H. Kurz, J. Phys.: Condens. Matter **18**, S601 (2006).
[22] R. Mendis, V. Astley, J. Liu, and D. M. Mittleman, Appl. Phys. Lett. **95**, 171113 (2009).
[23] R. Mendis and D. Grischkowsky, Opt. Lett. **26**, 846 (2001).
[24] M. Mbonye, R. Mendis, and D. M. Mittleman, Appl. Phys. Lett. **100**, 111120 (2012).
[25] J. Deibel, M. Escarra, N. Berndsen, K. Wang, and D. Mittleman, Proc. IEEE **95**, 1624 (2007).
[26] S. I. Bozhevolnyi, V. S. Volkov, E. Devaux, and T. W. Ebbesen, Phys. Rev. Lett. **95**, 046802 (2005).
[27] S. I. Bozhevolnyi, V. S. Volkov, E. Devaux, J.-Y. Laluet, and T. W. Ebbesen, Nature (London) **440**, 508 (2006).
[28] C. Bonnet, D. Chauvat, O. Emile, F. Bretenaker, A. Le Floch, and L. Dutriaux, Opt. Lett. **26**, 666 (2001).
[29] X. Yin, L. Hesselink, Z. Liu, N. Fang, and X. Zhang, Appl. Phys. Lett. **85**, 372 (2004).
[30] M. Merano, A. Aiello, G. W. t'Hooft, M. P. van Exter, E. R. Eliel, and J. P. Woerdman, Opt. Express **15**, 15928 (2007).
[31] R. F. Gragg, Am. J. Phys. **56**, 1092 (1988).